JOURNAL OF GEOPHYSICAL RESEARCH, VOL. 96, NO. C6, PAGES 10,617–10,624, JUNE 15, 1991

Ice Motions Forced by Boundary Layer Turbulence

R. L. DIMARCO, J. P. DUGAN, AND W. W. MARTIN

Arete Associates, Arlington, Virginia

The motions of ice on frozen oceans in the frequency band from 0.05 to 10.0 s^{-1} have typically been associated with surface gravity waves which were generated by distant storms in the open ocean and which then propagate into the ice. Evidence relating these motions to local wind forcing has been less direct. Data on ice motions have been obtained with tilt meters on a land-locked, frozen lake, and the motions are shown to be directly related to forcing by the local wind. The variance of ice surface tilt increased by more than 3 orders of magnitude when the mean wind speed increased by a factor of less than 2, even when the wind speed remained below the minimum phase speed for freely propagating waves. A model is presented in which ice motions result from an interaction between turbulent eddies in the atmosphere and the ice surface. Model predictions are shown to be consistent with the lake observations.

1. INTRODUCTION

Surface ice motion energy in the ice-covered ocean at frequencies below 10.0 s^{-1} has typically been ascribed to the propagation of surface gravity waves from the open ocean into pack ice and ice shelves [*Hunkins*, 1962; *LeSchack and Haubrich*, 1964; *Williams and Robinson*, 1981]. A number of studies have examined the propagation of these waves [*Robin*, 1963; *Wadhams*, 1973; *Williams and Robinson*, 1981] and have shown that they are generated by wind outside the ice covered area and then propagate into the ice. The waves are attenuated preferentially at high frequencies, while the low-frequency components attenuate slowly enough that they are measurable at distant locations. However, both Hunkins and LeSchack and Haubrich ascribe some motions to the local wind, while *Bogorodskiy* [1982] and *Bates and Shapiro* [1980] attribute a portion of the energy to ridge-building events. The evidence presented by Hunkins for the relation to local wind is that the level of ice wave energy increased considerably at times when the wind speed was above about 10 to 12 m s^{-1}. In addition, he points out that the minimum phase speed which occurs in the dispersion relation for flexural-gravity waves could account for a threshold wind speed for efficient (i.e., resonant) wave generation. The concept of wave generation above the phase speed minimum is further developed by *Davys et al.* [1985]. LeSchack and Haubrich also noted possible effects of local wind in their data, although the conclusion is only weakly supported by the published data. More recently, *Squire* [1986] and *Crocker and Wadhams* [1988] have inferred local wave generation by wind from strain meter data. In both cases, measurable ice deformations were observed at wind speeds well below the minimum phase speed of freely propagating flexural-gravity waves. These authors in both cases invoke the model of *Mills* [1972], in which the waves arise from an (apparent) oscillating force which translates downwind at the mean wind speed. This model is capable of producing ice motions at any wind velocity, with a significant increase expected when the mean wind speed exceeds the wave group velocity.

This explanation of the observations is not very satisfying on several counts. First, the model for the wind fluctuations is not based upon known facts about the surface pressure under the atmospheric turbulent boundary layer. For example, it is not clear just how the fluctuating forces are related to the mean wind speed either in magnitude or in frequency content. Second, it would be useful if the model could predict the level of motion, or at least the functional dependence of the level upon the wind speed or the ice structural parameters.

In order to improve upon this situation, we have made limited measurements on an ice-covered lake to test the hypothesis of local generation of ice motions by the wind. The ice fully covered the lake, and with no boundary open to the sea, swell could not propagate in from distant storms. Also, without the large-scale compressive forces which often occur in pack ice, there were no ridge-building events. Thus any motions which were observed were most likely due to the local wind. The specific objective of the experiment was to determine the relationship between motions of the ice and the local wind. The observations suggest a simple model of the motions, which is presented in the next section. The instrumentation and experiment are discussed in section 3, and the observations are discussed in section 4.

2. THEORY

The modeling is directed toward the response of a floating ice sheet of uniform properties and infinite extent over deep water when it is subjected to forcing by the varying pressure associated with a turbulent wind. The ice is modeled in the familiar way as a floating, uniform, thin plate. The conceptual model of the atmospheric forcing is a set of independent pressure fluctuations, each applying a force normal to the surface of the ice. It is assumed that the turbulence is consistent with the Taylor hypothesis [*Taylor*, 1938; *Mizuno and Panofsky*, 1975], in which the turbulent eddies are advected downwind at the mean speed of the flow, essentially without change over some finite coherence time. In this case the advection speed is the mean wind speed, and we assume that the surface pressure fluctuations are advected downwind with these turbulent eddies. The degree to which the fluctuations are frozen with the flow has been a subject of considerable observational work in wind tunnel boundary layers [*Willmarth and Wooldridge*, 1962; *Wills*, 1970] and in

Paper number 91JC00786.
0148-0227/91/91JC-00786$05.00

the atmosphere [*Panofsky et al.*, 1974; *Perry et al.*, 1978; *Kristensen*, 1979]. For example, Wills exhibits the two-dimensional spectrum of pressure fluctuations in the frequency–downwind wavenumber regime, and the dominant effect is the advection due to the mean wind speed in the tunnel. The lowest-wavenumber fluctuations in the wall pressure are advected at nearly the free stream velocity, while higher-wavenumber fluctuations are advected at the lower mean velocity near the wall. The temporal bandwidth (half power level) is less than 50% of the measured frequency at the peak, so the spread about the local mean speed is not very large. The combined results of the laboratory and the atmospheric measurements lead to the conclusion that there is a well-defined band of energy along a line in the frequency-wavenumber spectrum which is near the wind speed. Thus to a good approximation, there is a very simple relationship between the frequency spectrum at a point and the downwind wavenumber spectrum of the pressure fluctuations.

The equations of motion to be described in the following also will require the downwind component of the spatial structure of these pressure fluctuations, and this will be specified through the above relationship with the frequency spectrum. The frequency spectrum of the surface pressure in the atmospheric boundary layer has been measured over land [*Gossard*, 1960; *Kimball and Lemon*, 1970; *Elliott*, 1972*a*; *Grachev and Mordukhovich*, 1988] and over water [*Elliott*, 1972*b*]. These measurements have shown that the spectra are well described by a power law in a frequency band broader than 10^{-2} to 10^{1} s^{-1}, which is the band of interest to our model. Although the spectra show some deviations from a straight line, notably around the integral scale of the turbulence, a single power law is a reasonable descriptor over the frequency band [e.g., *Gossard*, 1960, Figure 1]. The value of the spectral exponent obtained in the various investigations varied generally in the range of $-5/3$ to $-7/3$. Selecting a value in this range, we choose a spectral power law of ω^{-2}.

The ice is modeled as a uniform, thin plate floating on a fluid of infinite depth. The equation of motion for the sheet is then [*Nevel*, 1970; *Davys et al.*, 1985; *Schulkes and Sneyd*, 1988]

$$D\nabla^4\xi + \rho_I h \frac{\partial^2 \xi}{\partial t^2} = p - F(x, t) \qquad (1)$$

where ξ is the vertical deformation of the plate, D is the flexural rigidity, ∇^4 is the biharmonic operator, ρ_I is the ice density, h is the ice thickness, p is the ambient pressure at the surface ($z = 0$), and $F(x, t)$ is the external forcing. The terms on the left represent the force per unit area due to ice flexural rigidity and inertia of the plate. We take the flow in the ocean to be irrotational with velocity potential ϕ. By Bernoulli's theorem we then have

$$p = \rho \left.\frac{d\phi}{dt}\right|_{z=0} - \rho g \xi \qquad (2)$$

where g is the gravitational acceleration. Including the assumption of continuity and the condition that the flow does not cross the top ($z = 0$) or bottom ($z = H$) boundaries, we have

$$\nabla^2\phi + \frac{\partial^2\phi}{\partial z^2} = 0 \qquad (3)$$

$$\left.\frac{\partial\phi}{\partial z}\right|_{z=\xi} = \frac{\partial\xi}{\partial t} \qquad (4)$$

$$\left.\frac{\partial\phi}{\partial z}\right|_{z=H} = 0 \qquad (5)$$

We next take the spatial and temporal Fourier transforms of equations (2)–(5), solve (3) for ϕ, subject to (4) and (5), and then substitute into (2), yielding

$$p = \frac{\rho\omega^2\hat{\xi}}{k \tanh k(H - \hat{\xi})} - \rho g\hat{\xi} \qquad (6)$$

where $\hat{\xi}$ is the transformed deformation, ω is the angular frequency (in units of radians per second throughout), and k is the horizontal wavenumber in the downwind direction. If we assume that the water depth is much larger than the wavelength of the deformations, (6) reduces to

$$p = \frac{\rho\omega^2\hat{\xi}}{k} - \rho g\hat{\xi} \qquad (7)$$

Taking spatial and temporal Fourier transforms of (1), and inserting (7), we have the algebraic expression

$$[Dk^4 - \rho_I h\omega^2 + \rho g - \rho\omega^2/k]\hat{\xi} = \hat{F}(k, \omega) \qquad (8)$$

where $\hat{F}$ is the Fourier transform of the forcing function. The dispersion relation for freely propagating flexural-gravity waves is the solution of the homogeneous equation where the applied pressure is identically zero. The solutions of this homogeneous equation have been discussed a number of times previously [*Wadhams*, 1973; *Bates and Shapiro*, 1980; *Davys et al.*, 1985], and the dispersion curve is shown graphically in Figure 1 for the ice parameters appropriate to our experiment. Clearly visible in Figure 1*a* is a minimum in the phase speed. The slowest speed for all frequencies or wavelengths is typically referred to as the critical phase speed c_{cr}, and it is the speed for the onset of resonant interaction between a moving load and waves generated in the ice [*Eyre*, 1977; *Beltaos*, 1981; *Takizawa*, 1985]. The onset of the resonance is clear from the form of (8), as regular solutions of the inhomogeneous equation exist only for forcing functions which have finite amplitudes at frequency-wavenumber points disjoint from the solutions of the homogeneous equation. Thus wave generation on the ice due to the pressure fluctuations via the so-called Phillips mechanism [*Kinsman*, 1965] will occur only when the wind speed is equal to or greater than the minimum wave phase speed for which we would anticipate freely propagating waves. We refer to the frequency which corresponds to the phase speed minimum as the critical frequency ω_{cr}. At frequencies above the critical frequency (and hence at high wavenumbers), the flexural rigidity of the plate is the dominant restoring force for freely propagating waves, while below the critical frequency, gravity is the dominant force. At the lowest frequencies the finite lake depth causes the waves to be shallow water waves.

We have included in both Figure 1*a* and Figure 1*b* a line of constant wavenumber, with $k_c = 1/L_c(\mathrm{m}^{-1})$, where L_c is the characteristic length of the ice sheet. This is defined as

$$L_c = (D/\rho g)^{1/4} \qquad (9)$$

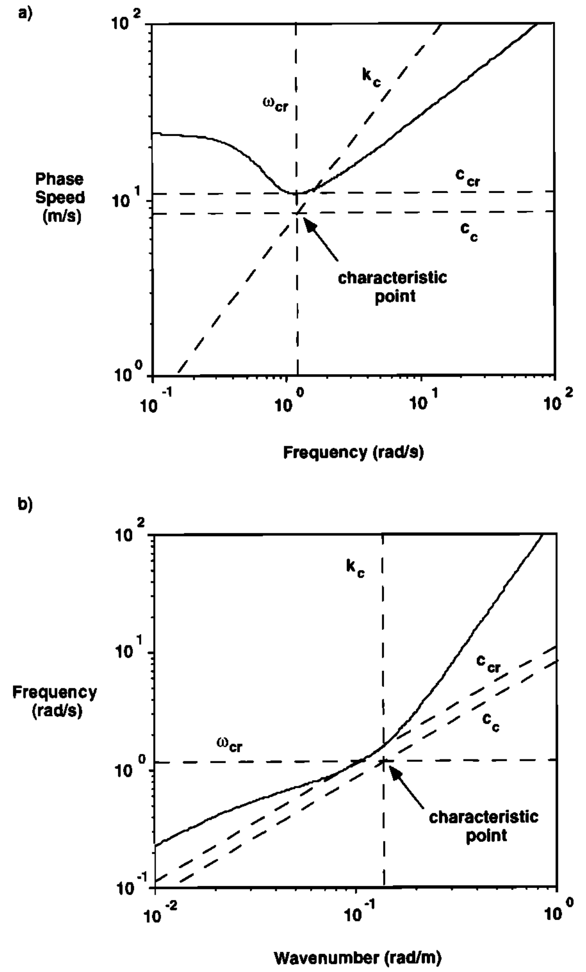

Fig. 1. Free wave dispersion relation for (*a*) phase speed versus frequency, and (*b*) frequency versus wavenumber, where ω_{cr} and c_{cr} are the critical frequency and phase speed and k_c and c_c are the characteristic wavenumber and phase speed; all of these quantities are defined in the text.

and represents the distance over which the ice will respond to a static deformation at a point [cf. *Nevel*, 1970; *Kerr*, 1976]. Under the conditions of this experiment the characteristic length is approximately 7.2 m. We will refer to the corresponding wavenumber, k_c, as the characteristic wavenumber. For wavenumbers smaller than k_c the gravity term in (8) is greater than the flexural term, while for larger wavenumbers the flexural term is the larger of the two. Also included in the plots of Figure 1 are two lines of constant phase speed. One of these is the critical phase speed, which intersects the dispersion curve at the critical frequency. The other constant phase speed line passes through the point of intersection between the critical frequency and the characteristic wavenumber. We refer to this phase speed as the characteristic phase speed c_c, and to the point of intersection as the characteristic point.

While the dispersion relation represents the homogeneous solution to (8), we are interested in the forced solutions. As was discussed previously, we assume that the ice is driven by the atmospheric pressure field associated with the boundary layer turbulence. The pressure is thus fluctuating over a broad frequency band, and length scales of the fluctuations range from much smaller than the ice characteristic length to much larger.

Spectra of pressure fluctuations have a reasonably constant slope in the frequency band of interest for this study, and we use the result of *Elliott* [1972*a*] to parameterize the slope

$$\omega S_p(\omega)\rho_a^{-2}u_*^4 \propto (\omega/U)^M \tag{10}$$

where $S_p(\omega)$ is the spectral density function of the atmospheric pressure fluctuations, ρ_a is the air density, u_* is the friction velocity, and U is the mean wind speed. Elliott finds $M = -0.7$, but we prefer to choose $M = -1$, yielding an ω^{-2} slope which, as we noted previously, is consistent with the bulk of the measured pressure data. The final result is not particularly sensitive to the specific value of this constant. If we set a proportionality constant β with units of inverse length and convert the friction velocity to measured wind speed via $U = \alpha u_*$, then we have

$$S_P(\omega) = \alpha^4\beta U^5\rho_a^2\omega^{-2} \tag{11}$$

We can use this forcing function in (8) to predict ice motion. Also, since the observations are of ice tilt rather than vertical displacement, we use $\xi_x = d\xi/dx \approx \xi k$ to change units. Squaring (8) and taking averages over the fluctuating parts, we have

$$\langle \hat{F}^2\rangle = [Dk^3 - \rho_I h\omega^2 k^{-1} + \rho g k^{-1} - \rho\omega^2 k^{-2}]^2\langle \xi_x^2\rangle \tag{12}$$

Or, in terms of spectral densities,

$$S_{\xi x}(\omega) = S_P(\omega)[Dk^3 - \rho_I h\omega^2 k^{-1} + \rho g k^{-1} - \rho\omega^2 k^{-2}]^{-2} \tag{13}$$

Using (11) for the forcing function along with Taylor's hypothesis, which allows us to set $k = \omega/U$, we have the ice tilt spectrum as

$$S_{\xi x}(\omega) = \alpha^4\beta\rho_a^2 U^5[DU^{-3}\omega^4 - \rho_I hU\omega^2 + \rho g U - \rho U^2\omega]^{-2} \tag{14}$$

Note that the only unmeasured quantities in this equation are the drag coefficient α and the proportionality constant β. This is a result that can be tested directly with measurements.

3. INSTRUMENTATION AND EXPERIMENT

The primary instrumentation for the field test of the model consisted of a two-axis tilt meter and an anemometer. The tilt meters were Sundstrand QA-1400 servo accelerometers, mounted as an orthogonal pair with the sensitive axes in the horizontal. In this configuration the observed variations in acceleration are due primarily to the tilt of the sensors with respect to the direction of gravity. The signal output actually is proportional to the sine of the tilt angle, but for the tilts involved the small angle approximation is valid. The sensor response is essentially constant from dc to 2 kHz, but since we are interested in relatively low frequencies, an antialias filter was set at 1 Hz and the sensors were sampled at 2 Hz. Figure 2 is a photo of the tilt meter mounting assembly. The mounting frame has a span of 22 cm, and support legs are frozen into the top of the ice. As implemented in this

Fig. 2. Photograph of the tilt meter measurement platform as mounted on the ice.

experiment, the resolution of the tilt meters was better than 1 μrad.

The anemometer was a UVW Gill-type, which was mounted at a height of 2 m. These data were also low passed at 1 Hz and sampled at 2 Hz. This sensor is typically used for turbulence measurements in the atmospheric boundary layer [*Busch et al.*, 1980], and the response time at typical wind speeds is about equal to the sampling interval.

These sensors were installed on seasonal ice on Newfound Lake in New Hampshire during the period February 11–13, 1987. Figure 3 is a map of the lake showing depth contours and the location of the instruments. This lake is surrounded by mountains with peaks as high as 520 m above the level of the lake. Both the tilt meter and the anemometer were aligned with one axis along the long axis of the lake.

The ice in the vicinity of the instruments was very uniform, and the measured ice thickness was 32 cm. About half of the ice surface had no snow cover, while the other half was covered with random drifts of snow which were up to 20 cm deep but generally less than 5 cm deep. We assume the surface temperature of the uncovered ice to be close to the air temperature which ranged from $-24°$ to $-13°$C during the period, while the snow-covered ice surface would be several degrees warmer. An appropriate Young's modulus for freshwater ice under these conditions would be 9 GPa [*Mellor*, 1983]. Our calculated value for the critical speed, shown in Figure 1, is 10.95 m s^{-1}, with a corresponding critical frequency of 1.17 s^{-1}. The characteristic length is 7.24 m, so the characteristic wavenumber is 0.138 m^{-1} and the characteristic speed is 8.47 m s^{-1}.

4. Observations

Figure 4 shows time series of the mean wind speed and the tilt variance during the period of midnight to noon on February 13. Both quantities were calculated in nonoverlapping 10-min intervals. Wind speeds ranged from calm to about 10 m s^{-1} and were generally increasing. The direction of the wind was within 20° of the long axis of the lake throughout the period; tilt variance is shown for the tilt meter aligned with that axis. The turbulence level of the wind (velocity variance) also increased throughout the period, with the rms velocity fluctuations remaining roughly 15% of the mean level. This result is consistent with other observations [e.g., *Eidsvik*, 1985], although rms levels in our observations are slightly higher.

The observed level of the tilt variance rose during the experiment in concert with the increase in the wind, as is

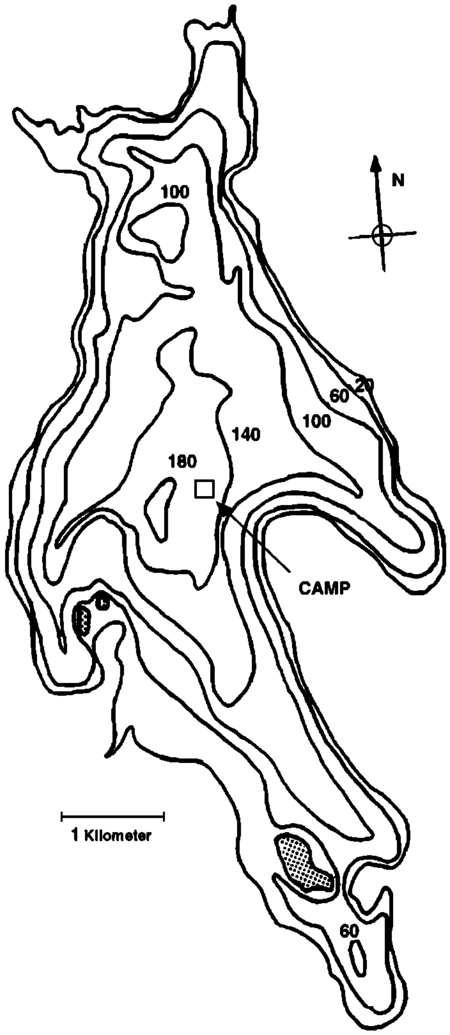

Fig. 3. Bathymetry in the Newfound Lake with the location of the measurements marked. Depths are in feet (1 foot = 0.3048 m).

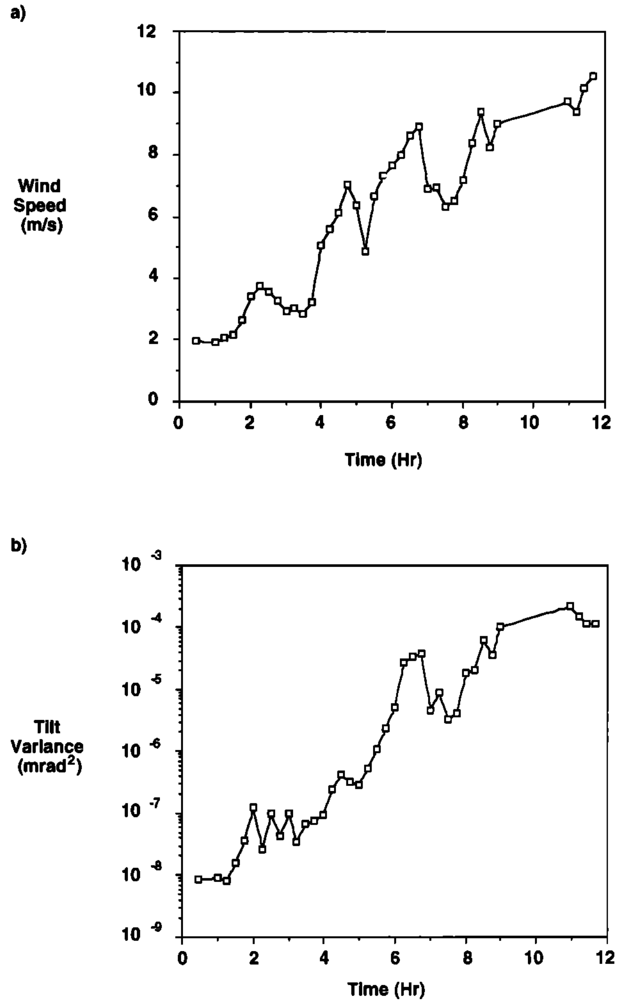

Fig. 4. Time history from midnight to noon on February 13, 1987, of (*a*) wind speed and (*b*) downwind tilt variance. Values shown are averages in nonoverlapping 10-min intervals.

shown in Figure 4. Figure 5 shows the tilt variance plotted as a function of the mean wind (10-min averages). Two regions with apparently different relationships between the tilt variance and the wind speed are evident in this figure; a lower-wind-speed region with a comparatively weak increase in tilt variance with increasing wind speed, and a higher-wind-speed region with a much stronger dependence of tilt upon mean wind. The differences in the apparent wind speed dependence leads us to anticipate that two distinct physical processes are dominant, depending upon the wind speed. Figure 5 also shows approximate fits to the data in the two regions. The lower-wind region has been fit with a U^3 slope and the higher-wind region with a U^{11} slope, with the crossover point near a wind speed of 5.5 m s^{-1}. These values were chosen from the predictions of the model, which are described in more detail below.

Figure 6 shows several measured tilt spectra at different wind speeds along with the model predictions from (14). The ensemble spectra were obtained in 15-min periods from seven subsets of 256 points each. The amplitude of the model predictions was set by fixing the multiplicative constant, $\alpha^4\beta\rho_a^2 = 1.2 \times 10^{-6}$ kg^2 m^{-2}, in equation (14). The drag coefficient and air density can be estimated for the test conditions. However, the value of β, and hence the overall normalization of the spectra, remains arbitrary. Accordingly, we adjusted the constant to give a best fit to the data. Wind speeds for the model were set equal to the average speeds in 15-min intervals used to compute the observed spectra. These speeds are noted in the figure next to each pair of spectra. While the overall normalization is arbitrary, the shape of the spectra and the relative amplitudes for different wind speeds are determined by equation (14). There is good agreement between the data and the model for those features.

Several regions of interest in frequency space can be noted by examining Figure 6 and equation (14). The spectra for low wind speed cases are white at low frequencies, with a high-frequency cutoff which apparently depends upon wind speed. Although the choice of a "cutoff" frequency may be made somewhat arbitrarily, the 3-dB points for the lowest wind cases, when converted to a wavenumber using the Taylor hypothesis and the mean wind, correspond roughly to the characteristic wavenumber. At the low wind speeds, the cutoff frequency is below the critical frequency, so the location of the cutoff in ω-k space is controlled by the characteristic wavenumber. In the terms of Figure 1, the cutoff frequency occurs at the locus of the intersection of k_c

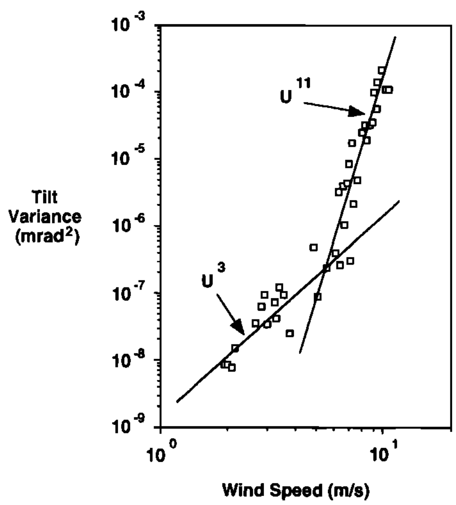

Fig. 5. Downwind tilt variance versus wind speed. The straight lines are eyeball best fits to the data with power laws consistent with the model.

with the wind speed, moving to higher frequencies with higher wind speeds. Examination of the relative sizes of the terms in (14) shows that at low wind speeds and low frequencies, the buoyancy term should dominate. This term has no frequency dependence, thus resulting in a white spectrum. At higher frequencies, with higher wavenumbers, the flexure of the plate becomes important, so the flexure term in (14) controls the behavior, leading to a cutoff at the characteristic wavenumber and an ω^{-8} roll-off, as is observed in Figure 6.

As the wind speed increases to the characteristic speed (but is still below the critical speed), the plate inertia and potential flow terms in (14) become important, and the response of the plate becomes more complicated. A distinct peak appears in the spectrum, between the buoyancy (white spectrum) and flexural (ω^{-8}) dominated regions. This peak appears at the critical frequency and, according to the model, will remain at the critical frequency until the wind reaches the critical speed. This leads to an interesting interpretation of Figure 1*a*. Note that the locus of points representing the frequency spectrum of the wind-driven forcing function is along a horizontal line located at the value of the wind speed. As the wind speed approaches the critical speed, those points along the frequency spectrum in the vicinity of the critical frequency are closest to the dispersion curve. It is these parts of the spectrum which are selectively enhanced as shown in Figure 6.

We now refer back to Figure 5, which compares the tilt variance with the average wind speed. For average wind speeds below c_c, where the spectrum does not exhibit a peak, the tilt variance is contributed primarily by the gravity term. From (14) we see that this term has a U^3 dependence, which is illustrated by a straight line drawn through the low-wind data in Figure 5. At higher wind speeds the variance comes mostly from the peak in the spectrum near the critical frequency. The height of this peak is determined by the flexural term which, according to the model, has a U^{11} dependence. We may compare this with the results in Figure 5 and note that when the average wind is greater than the characteristic speed the increase in tilt variance is in agreement with a slope of U^{11}, as is shown by the line drawn through the high-wind data. It is important to note that this large increase in variance with wind speed is still driven by boundary layer turbulence moving at a subcritical speed. The wind forcing is not on the dispersion curve, and thus the ice motions are not due to wave generation caused by resonant forcing of the ice. The results in Figures 5 and 6 are reasonable at all measured speeds, justifying the assumption

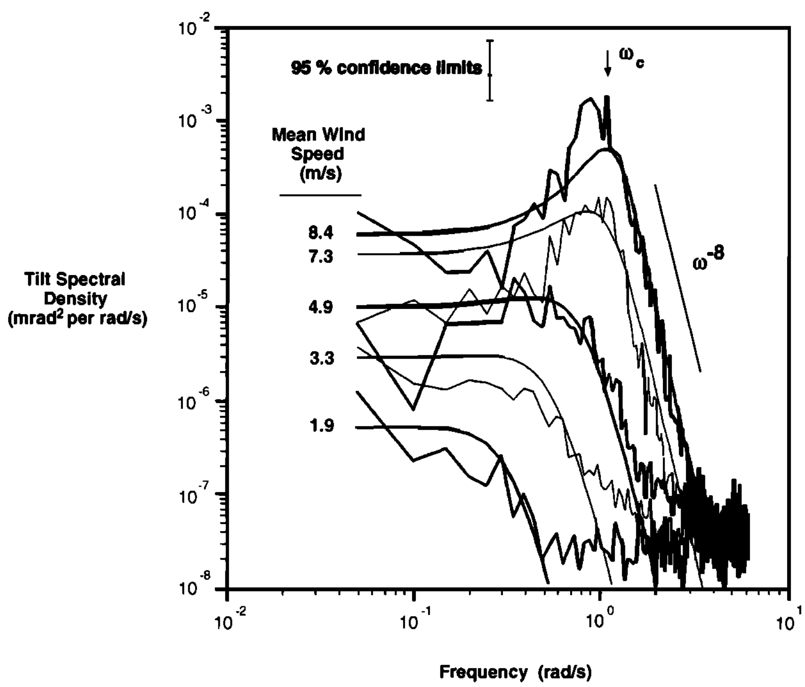

Fig. 6. Downwind tilt spectra for various wind speeds and model predictions for the same speeds. Speeds in meters per second are noted to the left of the spectral estimates. The ω^{-8} power law for $\omega > \omega_{cr}$ is shown for comparison. Curves for alternate wind speeds are shown in bold for clarity.

of a single, constant value of the drag coefficient. In addition, the low-frequency color of the tilt spectra in Figure 6 is in reasonable agreement with the model, thus justifying the assumption regarding the power law of the pressure spectrum. Small changes in the assumed power law do not appreciably affect the results.

We may now compare our model results with the observations of *Squire* [1986] and *Crocker and Wadhams* [1988]. The measurements in both of these cases were made with strain meters. The spectra in Figure 4 of Squire show similar behavior to those in our Figure 6, with an approximately white spectrum at low wind speeds and an increasingly prominent spectral peak at higher wind speeds. In his paper, Squire reported a critical speed of 15.2 m s^{-1} using a dynamic measurement technique. Since no characteristic speed was quoted, we used the ice parameters given and calculated a critical frequency of 0.72 s^{-1}, a critical speed of 13.2 m s^{-1}, and a characteristic speed of 8.0 m s^{-1}. Given the difference in these values of the critical speeds, the calculated characteristic speed may be slightly low, but this does not materially affect the comparison. Comparing spectral slopes is difficult because of the differences in the measurements. However, since tilts are a first spatial derivative of the vertical displacement while strain involves a second derivative, we may expect an additional factor of k for each term within the brackets in (14) for an equivalent strain expression. For the flexural rigidity term, shown to be dominant at high frequencies, this results in an expected roll-off of ω^{-10} for strain spectra. This is in good agreement with the spectra shown by Squire. The rate of increase in spectral level with wind speed observed by Squire is also in general agreement with our results.

The range of ice strengths observed by Crocker and Wadhams allow us to calculate a critical speed range of 13 to 19 m s^{-1} and a characteristic speed range of 8 to 14 m s^{-1}. The figures given by Crocker and Wadhams indicate a change in ice response at wind speeds below the lowest calculated critical speed but at or above the lowest characteristic speed, in agreement with our model. However, their observed rate of spectral increase with increasing wind speed is much lower than would be expected from our model and is also much lower than the corresponding rate of increase observed by Squire. We also note that while the location of the peak frequency observed by Crocker and Wadhams is about as we would expect, the behavior of the spectral peakedness, which declines with increasing wind speed above the characteristic speed, is at variance with both our observations and those of Squire. The cause of these differences is not evident from the available information. While the ice studied by Crocker and Wadhams was thicker than that of either Squire or this study, this is not expected to cause these discrepancies.

5. CONCLUSIONS

We have observed two regimes of ice response to wind-induced pressure fluctuations below the critical speed. Neither of these regimes shows ice motions to be the result of propagating waves. At low wind speeds the response is hydrostatic for low frequencies and flexural for high frequencies, with the cutoff frequency determined by the wind velocity and the characteristic length of the ice. The tilt spectrum is white below the cutoff frequency, and the tilt variance rises at a moderate rate with wind speed (U^3). When the wind velocity rises to a level at which this cutoff frequency is equal to the critical frequency, the ice response becomes more complicated. The variance of the ice response rises rapidly with wind speed (U^{11}), the spectrum is sharply peaked near the critical frequency, and it exhibits a rapid (ω^{-8}) high-frequency roll-off. A theory has been presented which accounts for these features through the local forcing of the ice sheet by a turbulent atmospheric boundary layer, without the generation of propagating waves in the ice sheet. Unfortunately, in this experiment, the wind speed did not exceed the critical speed, so this interesting situation has not been explored. In such a case, plate resonance and propagating wave modes would have to be included in the model.

While these observations were made on a freshwater lake, we must suspect that the same type of mechanism operates on sea ice. Refrozen leads or seasonal ice in fjords, with thin and relatively homogeneous ice, should be expected to behave in a manner very similar to the lake ice. Since the flexural rigidity increases as a cube of the thickness, multiyear floes are likely to have a sufficiently large critical speed as to never be subject to the U^{11} behavior. However, since the ice of a refrozen lead is typically well joined to that of the neighboring multiyear floe, the energy from disturbances generated over thin ice is expected to propagate some distance into the floe as waves of the same frequency, although the wavenumber would change to conform to the local dispersion relation for flexural-gravity waves. Regardless of the response of the thick ice, atmospheric forcing should be expected to contribute significantly to the motions of the thinner ice in this frequency band during periods of high wind, and it should produce a noticeable effect in the motion spectrum as noted by *Hunkins* [1962] and others.

Acknowledgments. This research was supported in part by the Arctic Sciences Program of ONR under contract N00014-90-C-0163, and the Scientific Officer, Tom Curtin, is gratefully acknowledged for his encouragement and support.

REFERENCES

Bates, H. F., and L. H. Shapiro, Long-period gravity waves in ice-covered sea, *J. Geophys. Res.*, *85*, 1095–1100, 1980.

Beltaos, S., Field studies on the response of floating ice sheets to moving loads, *Can. J. Civ. Eng.*, *8*, 1–8, 1981.

Bogorodskiy, V. V., Relaxation processes in arctic ice fields (in Russian), *Dokl. Akad. Nauk SSSR*, *250*, 24–26, 1982.

Busch, N. E., O. Christensen, L. Kristensen, L. Lading, and S. E. Larson, Cups, vanes, propellers, and laser anemometers, in *Air-Sea Interactions: Instruments and Methods*, edited by F. Dobson, L. Hasse, and R. Davis, pp. 11–46, Plenum, Press, New York, NY, 1980.

Crocker, G. B., and P. Wadhams, Observations of wind-generated waves in antarctic fast ice, *J. Phys. Oceanogr.*, *18*, 1292–1299, 1988.

Davys, J. W., R. J. Hosking, and A. D. Sneyd, Waves due to a steadily moving source on a floating ice plate, *J. Fluid Mech.*, *158*, 269–287, 1985.

Eidsvik, K. J., Large-sample estimates of wind fluctuations over the ocean, *Boundary Layer Meteorol.*, *32*, 103–132, 1985.

Elliott, J. A., Microscale pressure fluctuations measured within the lower atmospheric boundary layer, *J. Fluid Mech.*, *53*, 351–383, 1972*a*.

Elliott, J. A., Microscale pressure fluctuations near waves being generated by the wind, *J. Fluid Mech.*, *54*, 427–448, 1972*b*.

Eyre, D., The flexural motions of a floating ice sheet induced by moving vehicles, *J. Glaciol.*, *19*, 555–570, 1977.

Gossard, E., Spectra of atmospheric scalars, *J. Geophys. Res.*, *65*, 3339–3351, 1960.
Grachev, A., and M. Mordukovich, Spectrum of pressure fluctuations in the atmospheric ground layer, *Izv. Acad. Sci. USSR Atmos. Oceanic Phys.*, Engl. Transl., *24*, 159–161, 1988.
Hunkins, K., Waves on the Arctic Ocean, *J. Geophys. Res.*, *67*, 2477–2489, 1962.
Kerr, A. D., The bearing capacity of floating ice plates subjected to static or quasi-static loads, *J. Glaciol.*, *17*, 229–268, 1976.
Kimball, B., and E. Lemon, Spectra of air pressure fluctuations at the soil surface, *J. Geophys. Res.*, *75*, 6771–6777, 1970.
Kinsman, B., *Wind Waves*, 676 pp., Prentice-Hall, Englewood Cliffs, N. J., 1965.
Kristensen, L., On longitudinal spectral coherence, *Boundary Layer Meteorol.*, *16*, 145–153, 1979.
LeSchack, L. A., and R. A. Haubrich, Observations of waves on an ice-covered ocean, *J. Geophys. Res.*, *69*, 3815–3820, 1964.
Mellor, M., Mechanical behavior of sea ice, *Monogr. 83-1*, U.S. Army Cold Reg. Res. and Eng. Lab., Hanover, N. H., 1983.
Mills, D. A., On waves in a sea ice cover, *Res. Pap. 53*, 64 pp., Horace Lamb Cent. for Oceanogr. Res., Flinders Univ. of S. Australia, Bedford Park, Australia, 1972.
Mizuno, T., and H. A. Panofsky, The validity of Taylor's hypothesis in the atmospheric surface layer, *Boundary Layer Meteorol.*, *9*, 375–380, 1975.
Nevel, D. E., Moving loads on a floating ice sheet, *Rep. 261*, 15 pp., U.S. Army Cold Reg. Res. and Eng. Lab., Hanover, N. H., 1970.
Panofsky, H., D. Thomson, D. Sullivan, and D. Maravek, Two-point velocity statistics over Lake Ontario, *Boundary Layer Meteorol.*, *7*, 309–321, 1974.
Perry, S., J. Norman, H. Panofsky, and J. Martsolf, Horizontal coherence decay near large mesoscale variations in topography, *J. Atmos. Sci.*, *35*, 1884–1889, 1978.
Robin, G. de Q., Wave propagation through fields of pack ice, *Proc. R. Soc. London, Ser. A*, *255*, 313–339, 1963.
Schulkes, R. M. S. M., and A. D. Sneyd, Time-dependent response of floating ice to a steadily moving load, *J. Fluid Mech.*, *186*, 25–46, 1988.
Squire, V. A., Wind over ice: A mechanism for the generation of ice-coupled waves, in *Ice Technology, Proceedings of the First International Conference*, edited by T. K. S. Murthy, J. S. Conner, and C. A. Brebbia, pp. 115–128, Springer-Verlag, New York, 1986.
Takizawa, T., Deflection of a floating sea ice sheet induced by a moving load, *Cold Reg. Sci. Technol.*, *11*, 171–180, 1985.
Taylor, G. I., The spectrum of turbulence, *Proc. Roy. Soc. London, Ser. A*, *164*, 476–490, 1938.
Wadhams, P., Attenuation of swell by sea ice, *J. Geophys. Res.*, *78*, 3552–3563, 1973.
Webster, I. T., and R. W. Burling, A test of isotropy and Taylor's hypothesis in the atmospheric boundary layer, *Boundary Layer Meteorol.*, *20*, 429–443, 1981.
Williams, R. T., and E. S. Robinson, Flexural waves in the Ross Ice Shelf, *J. Geophys. Res.*, *86*, 6643–6648, 1981.
Willmarth, W. W., and C. E. Wooldridge, Measurements of the fluctuating pressure at the wall beneath a thick turbulent boundary layer, *J. Fluid Mech.*, *14*, 187–210, 1962.
Wills, J. A. B., Measurements of the wave-number/phase velocity spectrum of wall pressure beneath a turbulent boundary layer, *J. Fluid Mech.*, *45*, 65–90, 1970.

R. DiMarco (corresponding author), J. P. Dugan, and W. W. Martin, Arete Associates, P.O. Box 16287, Arlington, VA 22215.

(Received September 17, 1990;
revised February 27, 1991;
accepted October 13, 1990.)